ISSN 0038-0946, Solar System Research, 2016, Vol. 50, No. 1, pp. 13–23. © Pleiades Publishing, Inc., 2016.
Original Russian Text © V.V. Busarev, 2016, published in Astronomicheskii Vestnik, 2016, Vol. 50, No. 1, pp. 15–26.

New Reflectance Spectra of 40 Asteroids: A Comparison with the Previous Results and an Interpretation[1]

V. V. Busarev

Sternberg Astronomical Institute, Moscow Lomonosov State University, Moscow, 119991 Russia
e-mail: busarev@sai.msu.ru

Received April 22, 2014; in final form, May 28, 2015

Abstract—This paper presents and discusses selected reflectance spectra of 40 Main Belt asteroids. The spectra have been obtained by the author in the Crimean Laboratory of the Sternberg Astronomical Institute (2003–2009). The aim is to search for new spectral features that characterize the composition of the asteroids' material. The results are compared with earlier findings to reveal substantial irregularities in the distribution of the chemical-mineralogical compositions of the surface material of a number of minor planets (10 Hygiea, 13 Egeria, 14 Irene, 21 Lutetia, 45 Eugenia, 51 Nemausa, 55 Pandora, 64 Angelina, 69 Hesperia, 80 Sappho, 83 Beatrix, 92 Undina, 129 Antigone, 135 Hertha, and 785 Zwetana), which are manifest at different rotation phases. The vast majority of the analyzed high-temperature asteroids demonstrate subtle spectral features of an atypical hydrated and/or carbonaceous chondrite material (in the form of impurities or separate units), which are likely associated with the peculiarities of the formation of these bodies and the subsequent dynamic and impact processes, which lead, *inter alia*, to the delivery of atypical materials. Studies of 4 Vesta aboard NASA's *Dawn* spacecraft have found that asteroids of similar types can form their own phyllosilicate generations provided that their surface material contains buried icy or hydrated fragments of impacting bodies. The first evidence has been obtained of a spectral phase effect (SPE) at small phase angles ($\leq 4^\circ$) for 10 Hygiea, 21 Lutetia, and, possibly, 4 Vesta. The SPE manifests itself in an increasing spectral coefficient of brightness in the visible range with decreasing wavelength. This effect is present in the reflectance spectrum of CM2 carbonaceous material at a phase angle of 10° and absent at larger angles (Cloutis et al., 2011a). The shape of Hygeia's reflectance spectra at low phase angles appears to be controlled by the SPE during the most part of its rotation period, which may indicate a predominantly carbonaceous chondrite composition on a part of the asteroid's surface. For Vesta, the SPE may manifest itself in the flat or slightly concave shape of the asteorid's reflectance spectra at some of the rotation phases, which is likely caused by the increased number of dark spots on corresponding parts of its surface.

Keywords: asteroid spectrophotometry, mineralogy, surface material heterogeneities, spectral phase effect
DOI: 10.1134/S0038094616010019

INTRODUCTION

Measurements of the diffuse reflectance spectra of powders of natural crystalline materials or transmission spectra of their thin plates with a thickness ranging from tens of μm to ~1–2 mm (depending on the transparency of the sample) help identify the elemental and, in some cases, mineral composition of the samples. The latter is determined of the characteristic absorption bands of transition metals in the compound. These metals (Fe, Cr, Ti, etc.) have specific absorption bands in the visible and near infrared ranges due to a partly filled outer electron $3d^N$-shell (see, e.g., Adams, 1975; Platonov, 1976; Burns, 1993). The overall shape of the reflectance spectrum of all silicate compounds in the visible range is defined by the two strongest absorption bands of iron ions. The first such band (centered at 200 nm) is attributed to the ligand–metal charge transfer (the *ligands* are neutral molecules, ions, or radicals bonded with the central atom of the complex compound) (see, e.g., Loeffler et al., 1974). The second one (near 1000 nm) is generated by the spin-allowed electronic transitions in Fe^{2+} in the crystal field of major rock-forming minerals such as olivine (at 1010 nm), orthopyroxene (at 900 nm), and clinopyroxene (at 1000 nm) (Platonov, 1976; Burns, 1993). Additional indicators of these minerals in solid bodies may be weaker absorption bands centered at 506 nm (pyroxene) and 500 nm (olivine), which arise from the spin-forbidden electronic transitions in Fe^{2+} in the crystal field (Platonov, 1976; Khomenko and Platonov, 1987). As shown by theoretical and experimental studies, the more intensive ultraviolet band depends on the oxidation of silicate material and its long-wave wing determines the slope and shape of the reflectance spectrum of the solid body

[1] Full version of this paper is available via the SAI website: http://selena.sai.msu.ru/Bus/Publications/AB-15-1_Bus.pdf

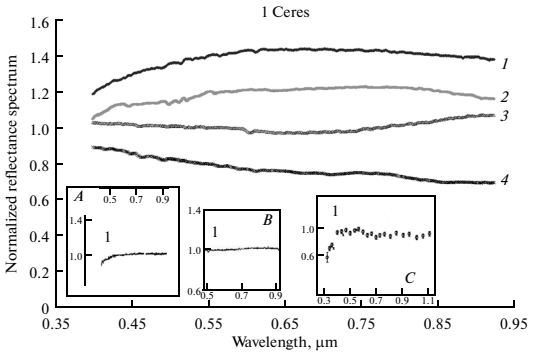
1 Ceres
Normalized reflectance spectrum
Wavelength, μm
1
2
3
4
A
B
C

(1)

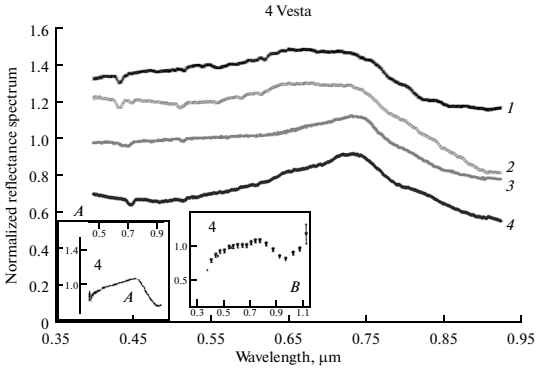
4 Vesta
Normalized reflectance spectrum
Wavelength, μm
1
2
3
4
A
B

(2)

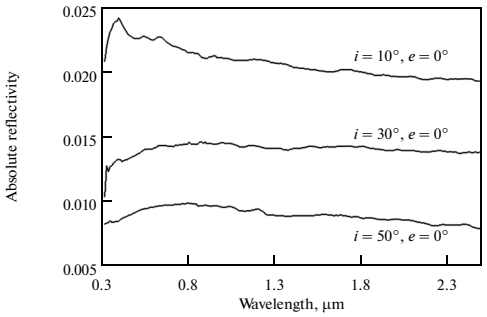
Absolute reflectivity
Wavelength, μm
i = 10°, e = 0°
i = 30°, e = 0°
i = 50°, e = 0°

(3)

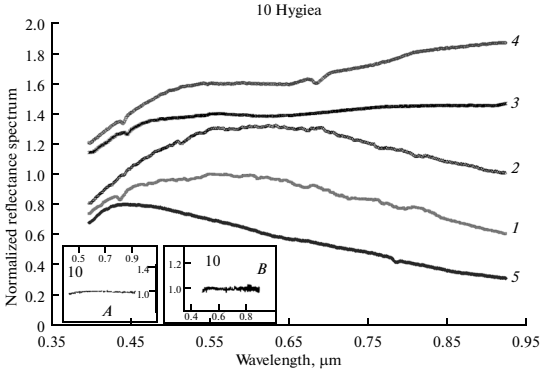
10 Hygiea
Normalized reflectance spectrum
Wavelength, μm
1
2
3
4
5
A
B

(4)

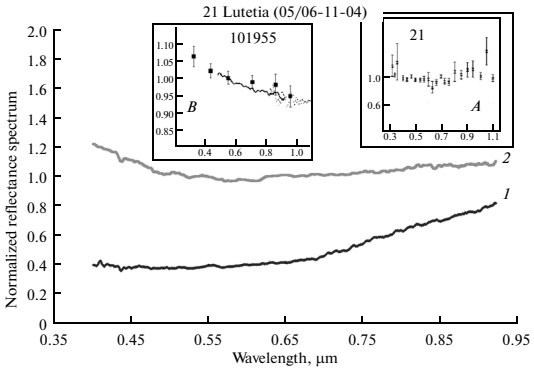
21 Lutetia (05/06-11-04)
Normalized reflectance spectrum
Wavelength, μm
101955
21
1
2
A
B

(5a)

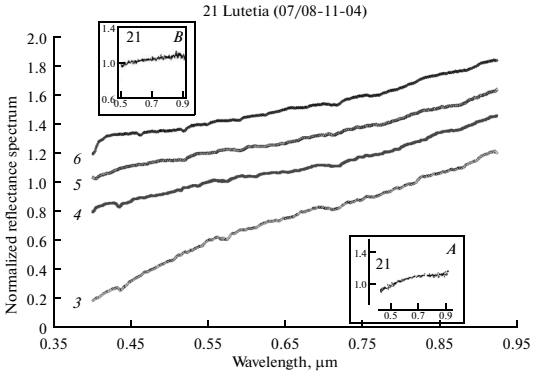
21 Lutetia (07/08-11-04)
Normalized reflectance spectrum
Wavelength, μm
3
4
5
6
21
A
B

(5b)

Figs. 1–8. Selected reflectance spectra of the observed asteroids (the spectra were normalized (by $\lambda = 0.5503$ μm) and arbitrarily shifted along the vertical axis for easy comparison) and similar data from other authors (all the reflectance spectra and the corresponding observational parameters of the asteroids are given in the full version of this paper at the SAI website: http://selena.sai.msu.ru/Bus/Publications/AB-15-1_Bus.pdf):

(1) The reflectance spectra of 1 Ceres (spectra *1–2* and *3–4* correspond to the diametrically opposite sides of the asteroid); the insets show the reflectance spectra of Ceres obtained in the surveys SMASS II (Bus and Binzel, 2002a) (*A*) and S^3OS^2 (Lazzaro et al., 2004) (*B*) and by Chapman et al. (1973) (*C*).

(2) The reflectance spectra of 4 Vesta obtained at a phase angle of ~4° (spectra *1–2* and *3–4* correspond to the diametrically opposite sides of the asteroid); inset *A* shows Vesta's reflectance spectrum from SMASS II (Bus and Binzel, 2002a) and inset *B* shows the one obtained by Chapman et al. (1973).

(3) The laboratory reflectance spectra of acid-insoluble components of the Murchison (CM2) meteorite at different phase angles (*i* is the angle of light incidence with respect to a normal to the plane of the sample; *e* is the angle of the direction in which the reflected light is detected; the particle size is 55–63 μm) (Cloutis et al., 2011a).

(4) The reflectance spectra of 10 Hygiea obtained at low phase angles (0.9°–2.6°) (spectra *1–2* and *5* were detected for the diametrically opposite orientations of the asteroid); insets *A* and *B* show Hygeia's reflectance spectra from the works (Bus and Binzel, 2002a) and Fornasier et al. (2014), respectively.

(5a and 5b) The reflectance spectra of 21 Lutetia obtained at low phase angles (2.5°–3.3°). Inset *A* in Fig. 5a shows Lutetia's reflectance spectrum obtained by Chapman et al. (1973); inset *B* shows that of the B-type asteroid 101955 Bennu (Hergenrother et al., 2013) from spectrometry data (Clark et al., 2011) (small dots, which merge into a solid line at wavelengths shorter than 0.9 μm) and ECAS-photometry data (Hergenrother et al., 2013) (squares). Insets *A* and *B* in Fig. 5b show the reflectance spectra of Lutetia from the surveys SMASS II (Bus and Binzel, 2002a) and S^3OS^2 (Lazzaro et al., 2004), respectively.

(6) The reflectance spectra of 64 Angelina; for comparison, insets *A* and *B* show Angelina's reflectance spectra from SMASS II (Bus and Binzel, 2002a) and (Fornasier et al., 2008), respectively.

(7) The reflectance spectra of 129 Antigone; insets *A* and *B* show Antigone's reflectance spectra from (Fornasier et al., 2010) and SMASS II (Bus and Binzel, 2002a), respectively.

(8) The reflectance spectra of 785 Zwetana; insets *A* and *B* show Zwetana's reflectance spectra from (Bus and Binzel, 2002a) and (Fornasier et al., 2010), respectively.

in the entire visible range (see, e.g., Loeffler et al., 1974; Burns, 1993). Previously, we showed that an Fe^{3+} indicator in low-Fe serpentines is an absorption band at 0.44 μm, the relative intensity of which can be as high as 25% (Busarev et al., 2004; 2008). There can also be rather strong absorption bands from the charge transfer between neighboring transition-metal cations. For example, in Fe-containing serpentines, these are $Fe^{2+} \rightarrow Fe^{3+}$ bands at 500–700 nm and 700–900 nm, or throughout the range 500–1000 nm (Calvin and King, 1997). These parameters depend on the relative positions of the cations in the crystal structure of the minerals, but the common feature is their large width of tens of nanometers or more (see, e.g., Platonov, 1976; Bakhtin, 1985). Relatively recently, scientists have discovered and partly investigated quite intensive absorption bands from magnetically interacting exchange-coupled pairs of cations of the same metal with the same or different valence in neighboring crystallographic positions. It was shown for Fe^{3+}-containing sapphire, hydrated sulfates, and tourmaline (Ferguson and Fielding, 1971; Rossman, 1975; Mattson and Rossman, 1984; Taran and Rossman, 2002) that the position of these bands (at 440, 490, 800–900, and 1100 nm) coincides with the spin-forbidden weak Fe^{3+} bands of the crystal field and their intensity may exceed that of the latter by two orders of magnitude.

A similar technique is used in remote sensing of asteroids and other solid atmosphereless celestial bodies on the basis of their diffuse reflectance spectra. The technique is described in detail in my previous publications (see, e.g., Busarev, 1999). Below is the description of selected reflectance spectra for 40 Main Belt asteroids, which are briefly discussed and compared with the results obtained by other authors.

SPECTRAL OBSERVATIONS OF ASTEROIDS: RESULTS AND DISCUSSION

The spectra were obtained at various times in 2003–2009 using a 1.25-m telescope of the Crimean Observatory with a spectrograph and CCD camera (SBIG ST-6) in the range 0.40–0.92 μm with a resolution of ~8 Å. The asteroids' ephemeris and other parameters at the times of observation and the measurement errors are listed in Table 1 in the full version of this paper, which is available via SAI website (http://selena.sai.msu.ru/Bus/Publications/AB-15-1_Bus.pdf).

Each spectrum was recorded consecutively in two wavelength ranges (0.40–0.67 and 0.65–0.92 μm, or *vice versa*) for a period from 10–15 min to 1.5 h, depending on the object's brightness. The initial processing of the observational data was performed using a standard software package for an SBIG ST-6 CCD camera. The data binding and wavelength scale calculation were based on hydrogen Balmer lines in the spectra of the primary standard α Lyr. The subsequent calculating and smoothing of the reflectance spectra of the asteroids and other transformations were performed using the standard software Excel and Origin. Along with the asteroids, we observed standard stars that are solar analogues in terms of their spectrophotometric parameters (16 Cyg B, HD 117176, and HD 10307) (Hardorp, 1980; Cayrel de Strobel, 1996). These stars were also used to determine the spectral

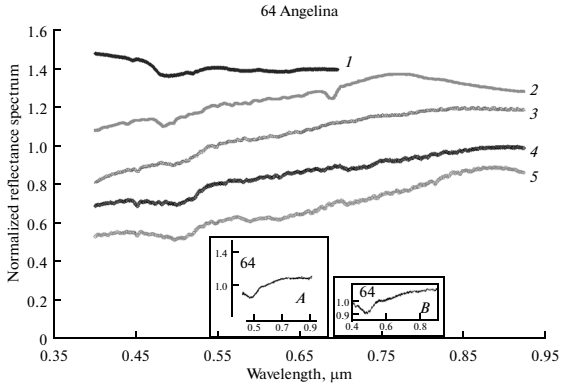

(6)

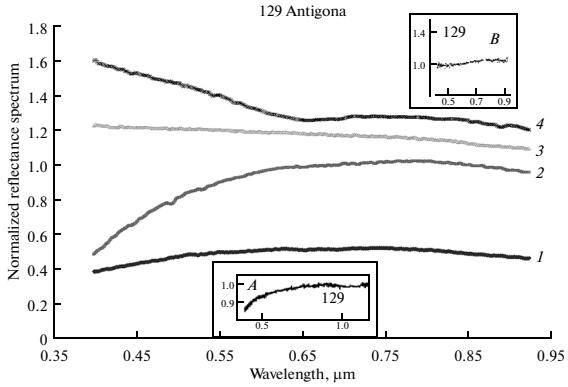

(7)

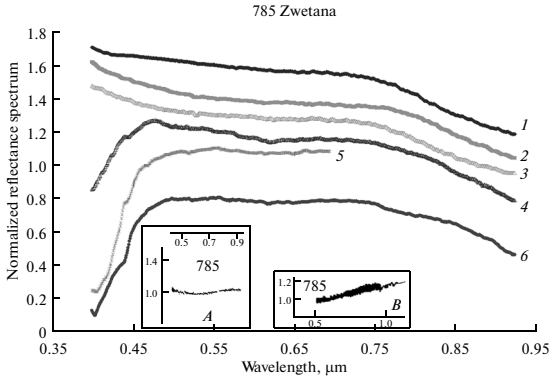

(8)

Fig. 1. (Contd.)

transparency function of the Earth's atmosphere for each observation night. The asteroids' reflectance spectra were calculated by the standard formula (Busarev, 1999). The reflectance spectra were smoothed (5-point running average) over the entire range to eliminate high-frequency noise. Near the boundaries of the spectral observation range (within about 500 Å) and residual telluric bands, a polynomial extrapolation, or approximation, was performed by the spectral continuum. Then, the reflectance spectrum of each asteroid was normalized by its reflectance value at the wavelength of 0.55 μm. The average relative standard errors of the reflectance spectra in the central part of the visible range are 1–2% and increase to 5–7% near the boundaries of the spectral range used in the study. In discussing each of the asteroids, we give in parentheses after the asteroid's name the following main parameters: rotation period (Batrakov et al., 2009), average geometric albedo (p_V), and diameter (D), which were calculated by the "standard" thermal model (Lebofsky et al., 1986) from the *IRAS* data (Tedesco et al., 2004), and the asteroids' spectral types (*Sp*) according to the taxonomic classifications proposed by Tholen (1989), Bus and Binzel (2002a; 2002b), and/or Bus–DeMeo (DeMeo et al., 2009), respectively. The parameters of Metis and Angelina were measured only in 1996 in the MSX experiment (Tedesco et al., 2002). The reflectance spectra are compared with the published results of other authors (Chapman et al., 1973; Bus and Binzel, 2002a; Lazzaro et al., 2004; Fornasier et al., 2008; 2010; 2011; 2014). However, the data published by Bus and Binzel (2002a), Lazzaro et al. (2004), and Fornasier et al. (2014) have limitations in the range 0.40–0.50 μm. In addition, these authors use different techniques for averaging the asteroids' reflectance spectra.

1 Ceres. This is the largest asteroid ($T_{rot} = 9.^h074$; $p_V = 0.113$; $D = 848.4$ km; *Sp* = G, C, C) and one of the dwarf planets (since 2006) according to the IAU classification. Ceres observations with *Hubble Space Telescope* (HST) were used to refine its mean geomet-

ric albedo, 0.090 (Li et al., 2006), and diameter, 974.6 × 909.4 km (Thomas et al., 2005). Our reflectance spectra for Ceres are generally consistent with its carbonaceous chondrite composition (Fig. 1) and with those obtained by other authors (Fig. 1, insets *A*, *B*, and *C*; adapted from Bus and Binzel (2002a), Lazzaro et al. (2004), and Chapman et al. (1973), respectively). However, it is the first time we have noticed that in visible light, some parts of Ceres' surface have a reflectance spectrum of a slightly convex shape (Fig. 1, spectra *1* and *2*) and other parts are characterized by a concave spectrum (Fig. 1, spectra *3* and *4*). This is confirmed by the spectrum obtained by Chapman et al. (1973) (inset *C*). Spectra *1–2* and *3–4* (Fig. 1) were obtained at relative rotation phases (RPs) corresponding to the diametrically opposite sides of the asteroid. For the purposes of this paper, we chose the RP of the first recorded spectrum as the zero RP. The change in the shape of Ceres' reflectance spectrum with rotation may indicate a different degree of hydration (or oxidation) of the surface material, which affects the intensity of the broadest intervalence absorption bands $Fe^{2+} \rightarrow Fe^{3+}$ in the visible range. A recent study (Perna et al., 2015) reports a weak absorption band centered at 0.67 μm, which is clearly seen in our spectrum *3* (Fig. 1). At present, Ceres is being explored by NASA's *Dawn* spacecraft. One of the first results was the discovery of marked color differences across the entire surface of the asteroid, which is evidence of a heterogeneous composition of the material (http://www.nasa.gov/jpl/pia19063/dawns-first-color-map-of-ceres/).

2 Pallas (see the description in http://selena.sai.msu.ru/Bus/Publications/AB-15-1_Bus.pdf).

4 Vesta. The third largest asteroid Vesta (T_{rot} = 5.^{h}342; $p_v = 0.423$; $D = 468.3$ km; *Sp* =V, V, V) is the brightest one among all the asteroids because its geometric albedo is greater by a factor of three to four than those of Ceres and Pallas, which exceed Vesta in size. The *HST* data helped refine Vesta's mean diameter, 530 km (Thomas et al., 1997). Vesta's reflectance spectra are shown in Fig. 2. The most notable spectral feature is a short-wavelength wing of the orthopyroxene absorption band at 0.90 μm, which is due to spin-allowed electronic transitions in Fe^{2+} ions in the M2 positions (see, e.g., Platonov, 1976). This interpretation is consistent with the presence of a weak pyroxene absorption band at 0.51 μm, which is due to spin-forbidden electronic transitions in Fe^{2+} ions (see, e.g., Platonov, 1976). The high intensity of the absorption band at 0.90 μm in the reflectance spectra of Vesta is evidence of a predominantly high-temperature (basalt) mineral composition of its surface material, which is dominated by orthopyroxene. At the same time, the spectra have a weak Fe^{3+} absorption band at 0.43–0.45 μm (~5–7%), which can be attributed to the presence of serpentine-type hydrosilicates in the surface material. In the range 0.40–0.65 μm, there are also differences in the shape of the continuum (Fig. 2), which changes from a sloping (curve *1*) to slightly concave one (curves *2* and *3*). The reflectance spectra *1–2* and *3–4* were obtained for the opposite orientations of the asteroid. The latter also have a sharper peak at 0.73 μm, a weak (~3–4%) Fe^{3+} absorption band shifted towards 0.44–0.45 μm, and a weak pyroxene (Fe^{2+}) band at 0.51 μm. A common feature of the reflectance spectra *2* (RP = 0.133) and *4* (RP = 0.694) is their slightly concave shape at 0.45–0.65 μm, which is typical of hydrated silicates and CI–CM carbonaceous chondrites (see, e.g., Busarev and Taran, 2002; Cloutis et al., 2011a; 2011b). Figure 2 shows Vesta's reflectance spectrum from the SMASS II survey (Bus and Binzel, 2002a) (inset *A*) and its reflectance spectrum from an earlier work (Chapman et al., 1973) (with a flat continuum at 0.55–0.70 μm) (inset *B*), which are consistent with our spectra.

It should be noted that Vesta was observed at small phase angles (~4°). It is therefore likely that in the range 0.40–0.65 μm, the shape of the reflectance spectra *2–4* (Fig. 2) is influenced by an SPE-type effect owing to the presence of numerous dark spots on the asteroid's surface, which were detected by *Dawn* (see, e.g., McCord et al., 2012). The SPE (spectral phase effect) was discovered during laboratory measurements of the reflectance spectra of acid-insoluble components of the matrix of the Murchison (CM2) carbonaceous chondrite at small phase angles (≤10°). The effect manifests itself in the unusual shape of the reflectance spectrum with a negative gradient in the entire visible range (Fig. 3) (Cloutis et al., 2011a). So far, there is no theoretical knowledge about the SPE origin (see, e.g., Petrova and Tishkovets, 2011), but it may be associated with the features of the opposition effect in dark-colored materials.

The obtained spectral characteristics of Vesta were fully confirmed during its detailed space exploration by *Dawn* in 2011 and can be interpreted as follows. Although Vesta has a high-temperature magmatic nature, there are numerous dark spots and hydrated formations on its predominantly basaltic surface (McCord et al., 2012; De Sanctis et al., 2012), which had likely appeared owing to impacts of primitive (carbonaceous chondrite and icy) bodies. It turned out that the spectral characteristics of the dark material on Vesta correspond, on average, to a mineral mixture of 80 wt % pyroxene (eucrite) and 20 wt % CM2 carbonaceous chondrite (Reddy et al., 2012). An earlier indication of the presence of carbonaceous chondrite material on Vesta was the discovery of inclusions of this material in HED-meteorites, which might be Vesta's fragments (Duke and Silver, 1967; Drake, 1979; Zolensky et al., 1996).

6 Hebe (see the description in http://selena.sai.msu.ru/Bus/Publications/AB-15-1_Bus.pdf).

7 Iris (see the description in http://selena.sai.msu.ru/Bus/Publications/AB-15-1_Bus.pdf).

8 Flora (see the description in http://selena.sai.msu.ru/Bus/Publications/AB-15-1_Bus.pdf).

9 Metis (see the description in http://selena.sai.msu.ru/Bus/Publications/AB-15-1_Bus.pdf).

10 Hygeia. Asteroid 10 Hygeia (T_{rot} = 27.^{h}623; p_v = 0.072; D = 407.1 km; *Sp* = C, C, C) is known to be the largest C-type asteroid. Two of its reflectance spectra (Fig. 4, curves *1* and *2*; RP = 0.00–0.21) were obtained by us with a small time difference (about one and a half hours); therefore, the differences between the spectra are within the error limit. However, the shape of the reflectance spectra is not consistent with the taxonomic (spectral) type of Hygeia, which corresponds to low-temperature mineralogy (see, e.g., Gaffey et al., 1989). Based on these data, we previously suggested that the changes in the shape of Hygeia's reflectance spectrum with rotation might be due to local dehydration of its surface material because of large impact events (Busarev, 2011). Spectra *3* and *4* (Fig. 4) were also recorded with a small time difference (about one hour) at RP = 0.34–0.38. They are consistent with the assigned spectral type and confirmed by the spectra obtained by other authors, which are given in insets *A* (Bus and Binzel, 2002a) and *B* (Fornasier et al., 2014) in Fig. 4. In spectra *3* and *4*, a weak absorption band at 0.44–0.45 μm (Fe^{3+}) (Busarev et al., 2008) confirms the low temperature mineralogy of the asteroid's material. Spectrum *4* (Fig. 4) at 0.68 μm shows a residual O_2 telluric band *B* (Kurucz, 2005). The last reflectance spectrum (Fig. 4, curve *5*) refers to the opposite side of Hygeia (RP = 0.56). It has a negative gradient in the entire visible range (as in B-type asteroids) and is very different from Hygeia's spectra recorded at other RPs. However, it was obtained at an extremely low phase angle of the asteroid, only 0.9°. Note that all the reflectance spectra shown in Fig. 4 correspond to low phase angles: φ = 2.6° for *3* and *4*; φ = 1.7° for *1* and *2,* and φ = 0.9° for *5*. They are numbered in a chronological order, but arranged in Fig. 4 (from bottom to top) in the order of increasing phase angle. Evidently, the gradual change in the shape of the asteroid's reflectance spectrum follows the same pattern. The difference in the magnitude of the gradient between the laboratory reflectance spectrum of CI carbonaceous chondrite, ~12% (Fig. 3, upper curve, φ = 10°) (according to Cloutis et al., 2011a), and that of Hygeia, ~50% (Fig. 4, curve *5*, φ = 0.9°), in the range 0.45–0.80 μm is likely due to the substantial difference in the phase angles. Thus, we have likely observational evidence that the shape of Hygeia's reflectance spectra at low phase angles is determined by the SPE. Moreover, since all of Hygeia's reflectance spectra were obtained at low phase angles and different rotation phases, we can assume a carbonaceous chondrite composition for a large part of its surface. This means that the SPE can be used as a new indicator of these substances on solid celestial bodies.

11 Parthenope (see the description in http://selena.sai.msu.ru/Bus/Publications/AB-15-1_Bus.pdf).

12 Victoria (see the description in http://selena.sai.msu.ru/Bus/Publications/AB-15-1_Bus.pdf).

13 Egeria (see the description in http://selena.sai.msu.ru/Bus/Publications/AB-15-1_Bus.pdf).

14 Irene (see the description in http://selena.sai.msu.ru/Bus/Publications/AB-15-1_Bus.pdf).

16 Psyche (see the description in http://selena.sai.msu.ru/Bus/Publications/AB-15-1_Bus.pdf).

18 Melpomene (see the description in http://selena.sai.msu.ru/Bus/Publications/AB-15-1_Bus.pdf).

21 Lutetia. The reflectance spectra of Lutetia (T_{rot} = 8.^{h}166; p_v = 0.221; D = 95.8 km; *Sp* =M, Xk, Xc) *1–6* (Figs. 5a and 5b) are given in the chronological order and cover the asteroid's entire rotation period. They provide evidence of a large variability in the asteroid's spectral characteristics (from M–S to F–B-types) and, probably, of a composition ranging from high-temperature (olivine–pyroxene) and/or incorporating metallic iron to carbonaceous chondrite. According to some authors (Ockert-Bell et al., 2010), Lutetia's reflectance spectrum in the range 0.4–2.4 μm averaged over its rotation period has a convex shape and no absorption bands of high-temperature minerals at 0.9 and 1.9 μm. However, this does not agree with the reflectance spectra *1* and *2* (Fig. 5a), which we obtained at close RP values (0.000–0.025) for Lutetia. They have a shape varying from flat to concave with a negative gradient in the blue part, which is typical of primitive F–B-asteroids. Previously, we noted (Busarev, 2010) that this shape of reflectance spectra is typical of hydrosilicate enriched carbonaceous chondrites due to light absorption $Fe^{2+} \rightarrow Fe^{3+}$ charge transfer in the crystal structure. Another indicator of the presence of Fe^{3+} is a weak absorption band at 0.43–0.45 μm (Fig. 5a) (Busarev et al., 2008). The reliability of these spectral features of Lutetia is confirmed by the previous data (Chapman et al., 1973) (Fig. 5a, inset *A*). The same figure (inset *B*) shows, for comparison, the reflectance spectrum of the B-type asteroid 101955 Bennu (Hergenrother et al., 2013), which is compelling evidence that some asteroids really have these spectral characteristics. Experimental simulations revealed these properties in the fractured material (with a particle size of <125 μm) of the Ivuna (CI) meteorite heated to 700°C (Clark et al., 2011; Cloutis et al., 2011a). The shape of the reflectance spectra *1* and *2* of Lutetia (Fig. 5a) may be influenced by the SPE because they were obtained at a phase angle of 2.5°. Spectra *1* and *2* are likely to correspond to that part of the asteroid surface, which is covered with carbonaceous chondrite and/or hydrated substance, as evidenced by the detected spectral features. Although all the reflectance spectra of Lutetia (*1–6*) were obtained at small phase angles (2.5°–3.3°), only spectra *1* and *2* show SPE signatures (Fig. 5a). A largely different shape (with a substantial positive gra-

dient) is observed for the reflectance spectra *3–6* of Lutetia (Fig. 5b), which correspond to its diametrically opposite side (RP = 0.545–0.585). These spectra are similar in shape to those of S-type asteroids although they show no signs of a pyroxene–olivine absorption band at 0.9 μm. Taking into account that Lutetia has a relatively high geometric albedo (0.22), we can assume a predominantly high-temperature composition for its material. However, some features in these spectra are weak absorption bands at 0.43–0.45 μm (Fe^{3+}) and 0.52 μm (Fe^{2+}) and an absorption band at 0.71–0.72 μm ($Fe^{2+} \rightarrow Fe^{3+}$?) which can be signs of the presence of hydrated or oxygenated compounds in the surface material. The reflectance spectra *3–6* are consistent with those of Lutetia from (Bus and Binzel, 2002a) and (Lazzaro et al., 2004), which are given in Fig. 5b, insets *A* and *B*, respectively. Substantial variations in the shape and slope of Lutetia's reflectance spectrum with rotation in the range 0.53–0.80 μm, which correspond to the C–X-types, were also detected by Italian and French researchers (Lazzarin et al., 2010). Furthermore, the presence of water in a bound state on the surface of Lutetia was ascertained from an absorption band at 3 μm in its reflectance spectrum (Rivkin et al., 2000).

23 Thalia (see the description in http://selena.sai.msu.ru/Bus/Publications/AB-15-1_Bus.pdf).

29 Amphitrite (see the description in http://selena.sai.msu.ru/Bus/Publications/AB-15-1_Bus.pdf).

43 Ariadne (see the description in http://selena.sai.msu.ru/Bus/Publications/AB-15-1_Bus.pdf).

45 Eugenia (see the description in http://selena.sai.msu.ru/Bus/Publications/AB-15-1_Bus.pdf).

51 Nemausa (see the description in http://selena.sai.msu.ru/Bus/Publications/AB-15-1_Bus.pdf).

55 Pandora (see the description in http://selena.sai.msu.ru/Bus/Publications/AB-15-1_Bus.pdf).

64 Angelina. The reflectance spectra of Angelina that were obtained during two nights (T_{rot} = 8.^{h}752; p_v = 0.405; D = 61.4 km; Sp = E, Xe, Xe) (Fig. 6) cover about a quarter of its rotation period and are consistent with its classification. They show weak absorption bands in the short wavelength region, a more intensive band at 0.49 μm, and episodic bands at 0.60 μm and close to 0.75 μm (Fig. 6). A typical feature of these types of asteroids is the dominance of the high-temperature mineral enstatite (Fe-free magnesium pyroxene) in their substance (see, e.g., Gaffey et al., 1989). By studying the mineral analogues, Angelina was more accurately classified as an E(II)-subtype asteroid, which is characterized by a visible absorption band at 0.49 μm (due to the small amount of Fe^{2+}), typical of oldgamite or calcium sulfide (CaS) (Gaffey and Kelley, 2004). This band is present in all of Angelina's reflectance spectra obtained by us and those obtained by other authors, which are given in insets *A* (Bus and Binzel, 2002a) and *B* (Fornasier et al., 2008) in Fig. 6. Noteworthy is the fact that our spectra of Angelina have weak absorption bands at 0.43–0.45 μm (Fig. 6). Fornasier et al. (2008) write about a high heterogeneity of Angelina's substance, but provide no arguments. The variability of the spectral and, hence, mineralogical properties of Angelina's surface is illustrated by our spectra *1* and *2* with gradients of the opposite sign at wavelengths shorter than 0.75 μm. Moreover, the data at 3 μm provide evidence of hydrosilicates on Angelina (Rivkin et al., 1995). This fact is confirmed by the slightly concave shape of the spectra in the range 0.55–0.75 μm ($Fe^{2+} \rightarrow Fe^{3+}$?) (curves *1* and *5*), which is typical of hydrosilicates, and weak bands at 0.43–0.45 μm (Fe^{3+}) in all the spectra (Fig. 6). It is also interesting that although Angelina is considered as a high-temperature asteroid (see, e.g., Gaffey and Kelley, 2004), its radar albedo is only 40% of that of 69 Hesperia, an asteroid with a predominantly metallic composition of the material (Shepard et al., 2010; 2011).

67 Asia (see the description in http://selena.sai.msu.ru/Bus/Publications/AB-15-1_Bus.pdf).

69 Hesperia (see the description in http://selena.sai.msu.ru/Bus/Publications/AB-15-1_Bus.pdf).

80 Sappho (see the description in http://selena.sai.msu.ru/Bus/Publications/AB-15-1_Bus.pdf).

83 Beatrix (see the description in http://selena.sai.msu.ru/Bus/Publications/AB-15-1_Bus.pdf).

92 Undina (see the description in http://selena.sai.msu.ru/Bus/Publications/AB-15-1_Bus.pdf).

115 Thyra (see the description in http://selena.sai.msu.ru/Bus/Publications/AB-15-1_Bus.pdf).

129 Antigone. This asteroid, like Thyra, has a high geometric albedo and even a shorter rotation period, which are consistent with Antigone's assigned spectral classes (T_{rot} = 4.^{h}9572; p_v = 0.275; D = 79.8 km; Sp = M, X) as a body with a mainly high-temperature composition of the material. However, we obtained reflectance spectra for Antigone in a wide range of RPs (Fig. 7), which demonstrate a great variety of shapes—from convex, as those published by Fornasier et al. (2010) (Fig. 11, inset *A*), to slightly concave, as those in the SMASS II survey (Bus and Binzel, 2002a) (Fig. 7, insert *A*). There could be signs of olivine: the weak absorption band at 0.50 μm (Fe^{2+} and Fe^{3+}?) in spectrum *2* (Fig. 7) and the short-wavelength wing of the absorption band at 1.0 μm (Fig. 7). The presence of hydrated compounds in the material is evidenced by weak details at 0.43–0.45 μm (Fe^{3+}) (spectra *2* and *4*) and a stronger absorption band at 0.65 μm ($Fe^{2+} \rightarrow Fe^{3+}$?) (spectrum *4*), along with a generally negative gradient. Evidence of hydrosilicates on Antigone was also found during its infrared observations at 3 μm (Rivkin et al., 2000).

135 Hertha (see the description in http://selena.sai.msu.ru/Bus/Publications/AB-15-1_Bus.pdf).

141 Lumen (see the description in http://selena.sai.msu.ru/Bus/Publications/AB-15-1_Bus.pdf).

196 Philomela (see the description in http://selena.sai.msu.ru/Bus/Publications/AB-15-1_Bus.pdf).

198 Ampella (see the description in http://selena.sai.msu.ru/Bus/Publications/AB-15-1_Bus.pdf).

230 Athamantis (see the description in http://selena.sai.msu.ru/Bus/Publications/AB-15-1_Bus.pdf).

250 Bettina (see the description in http://selena.sai.msu.ru/Bus/Publications/AB-15-1_Bus.pdf).

264 Libussa (see the description in http://selena.sai.msu.ru/Bus/Publications/AB-15-1_Bus.pdf).

349 Dembowska (see the description in http://selena.sai.msu.ru/Bus/Publications/AB-15-1_Bus.pdf).

532 Herculina (see the description in http://selena.sai.msu.ru/Bus/Publications/AB-15-1_Bus.pdf).

584 Semiramis (see the description in http://selena.sai.msu.ru/Bus/Publications/AB-15-1_Bus.pdf).

785 Zwetana. Our reflectance spectra of Zwetana ($T_{rot} = 8.^h8882$; $p_v = 0.125$; $D = 48.5$ km; Sp = M, Cb, Cb) (Fig. 8) are not consistent with its assigned spectral class M, if we proceed from the shape given in Tholen's classification (Tholen and Barucci, 1989). The latest classifications (Bus and Binzel, 2002b; DeMeo et al., 2009) assign Zwetana to the primitive Cb-class. The asteroid's reflectance spectra *1–3* (Fig. 8) have a negative gradient throughout the visible and near infrared ranges. Moreover, spectra *4* and *6* (Fig. 8), which were obtained for its almost diametrically opposite orientation, have a negative gradient at wavelengths shorter than 0.75 μm. The presence of oxidized and/or hydrated compounds is confirmed by the fact that spectra *4–6* have a weaker yet broader absorption band centered at 0.62 μm and a weak absorption band at 0.44 μm (Fe^{3+}). The variability of the composition of Zwetana's material is confirmed by differences in its reflectance spectra from other sources, which are presented in insets *A* (Bus and Binzel, 2002a) and *B* (Fornasier et al., 2010) in Fig. 8.

CONCLUSIONS

The comparison of our results for the asteroids' spectral characteristics with those of other authors shows that the main reason for the differences could be the heterogeneous chemical and mineral composition of the asteroids' surface material. These differences manifest themselves, as a rule, in inconsistencies of the rotation phases and aspect angles for the same objects observed at different times. In addition, it is necessary to take into account the general features of the ground-based observational data for asteroids. In ground-based observations, all asteroids appear as point objects, and their measured parameters are averaged over the entire visible portion of the surface. In particular, deviations in the composition of the asteroid's material can be detected during the object's rotation from variations in the normalized reflectance spectrum. However, as is known from variations in asteroids' brightness and from their space images, the vast majority of these bodies have an irregular shape, which can be approximated by a complex polyhedron. This means that an asteroid with an inhomogeneous surface composition and sufficiently rapid rotation is likely to have substantial variations in the reflectance spectra, even in the case of a small difference in RPs. These changes may be caused by a "jump" of the line of sight from one "face" of the asteroid to another with a different surface composition. Moreover, experience shows that spectral fluctuations may sometimes occur in the Earth's atmosphere even when the sky is clear, especially when the observed object has a large air mass. Therefore, suspicious data were excluded from consideration.

Thus, based on a critical review of the observational data obtained at different rotation phases of the asteroids, we can assert that signatures of substantial spectral and, probably, chemical and mineralogical heterogeneities of the surface material have been detected for 10 Hygiea, 13 Egeria, 14 Irene, 21 Lutetia, 45 Eugenia, 51 Nemausa, 55 Pandora, 64 Angelina, 69 Hesperia, 80 Sappho, 83 Beatrix, 92 Undina, 129 Antigone, 135 Hertha, and 785 Zwetana.

Another important result is the discovery of spectral signatures of hydrated silicates and/or Fe^{3+}-containing iron oxides (hydroxides) on the vast majority of the studied high-temperature asteroids. The earlier spectrophotometric measurements showed that the surface material of many high-temperature (S-, M-, E-, and V-type) asteroids includes Fe^{3+}-containing oxidized compounds and/or hydrosilicates (Rivkin et al., 1995; 2000; Busarev, 2002). If we assume from the generally accepted view of high-temperature (M-, S-, V-, E-, A-, and R-type) asteroids as bodies with a predominantly high-temperature mineralogy (see, e.g., Bell et al., 1989; Gaffey et al., 1989) that had experienced a heating to temperatures of ~1000–1500°C during their formation, this fact seems strange. As known from the Earth's mineralogy, the majority of hydrated silicates and Fe^{3+}-containing oxides and hydroxides are completely destroyed at temperatures of ~400–500°C (see, e.g., Betekhtin, 1951; Korzhinskii, 1957). Some quantity of Fe^{3+} could have remained in the asteroid's material in the case of an insufficiently strong or uneven heating during its primary thermal evolution, whose energy source was the decay of short-lived isotopes (mainly ^{26}Al). As shown by simulations (Grimm and McSween, 1993; McSween et al., 2002), the material of some of asteroids' parent bodies, especially on the periphery of the Main Belt, could have contained water ice. However, in the harsh space conditions, these compounds cannot exist on the surface of asteroids for a long time. Given the long and perpetual exposure to shortwave radiation and intense corpuscular and micrometeorite streams, these compounds should transform into more reduced ones. Furthermore, the space maturation of solid matter, which is caused by the same factors, leads

to the degradation of the crystal structure and its transition to an amorphous form with no distinct spectral signatures. The heterogeneity of asteroids' material may occur primarily due to the impact process because only a part of the material is processed during impact events and transfered (Busarev, 2002; 2011). When fragments of impacting icy bodies are buried in the surface material of high-temperature asteroids, they can form their own generation of hydrosilicates. This assumption is confirmed by the results of detailed studies of 4 Vesta by *Dawn* (NASA). Its predominantly basaltic surface has numerous spots of hydrosilicates and darker spots of carbonaceous chondrites (Reddy et al., 2012; De Sanctis et al., 2012), whose distributions coincide only partially.

As shown by laboratory measurements of the reflectance spectra of the CM2 carbonaceous chondrite substance (Cloutis et al., 2011a) at different phase angles, the shape of the reflectance spectrum of these materials is determined not only by composition, grain size, and particle structure and packing but also by an effect that is similar to the opposition one and occurs at phase angles of $\leq 10°$. We called it the *spectral-phase effect* (SPE). Apparently, we were able to detect this effect on 10 Hygiea, 21 Lutetia, and possibly on 4 Vesta. As shown in the discussion, it manifests itself in a sharp change in the sign (from positive to negative) of the gradient of the asteroid's reflectance spectrum continuum in the short-wave part of the spectrum or in the entire visible range at low phase angles. On Hygeia (Fig. 4) and Lutetia (Fig. 5a), the SPE was detected quite distinctly and appears to occur in the reflectance spectrum of that part of the asteroid that is covered with predominantly carbonaceous chondrite material. In the case of Vesta, an SPE signature may be the flat or somewhat concave shape of its reflectance spectra at some RPs (Fig. 2); this shape is likely due to the increased number of dark spots on the corresponding parts of Vesta's surface. Obviously, there is a need for new, more rigorous studies of the SPE in laboratory conditions. If this effect is proved to be universal for all or some of the groups of carbonaceous chondrites, it can be used as a new indicator of this substance on solid celestial bodies.

ACKNOWLEDGMENTS

The author would like to thank the anonymous reviewers for their critical comments and discussions of his results, which helped him largely improve the content of the paper.

REFERENCES

Adams, J.B., Interpretation of visible and near-infrared diffuse reflectance spectra of pyroxenes and other rock-forming minerals, in *Infrared and Raman Spectroscopy of Lunar and Terrestrial Minerals,* Karr, C., Ed., New York: Acad. Press, 1975, pp. 91–116.

Bakhtin, A.I., *Porodoobrazuyushchie silikaty: opticheskie spektry, kristallokhimiya, zakonomernosti okraski, tipomorfizm* (Rock-Forming Silicates: Optical Spectra, Crystal Chemistry, Coloring Regularities, Typomorphysm), Kazan: Kazan State Univ., 1985.

Bell, J.F., Davis, D.R., Hartmann, W.K., and Gaffey, M.J., The big picture, in *Asteroids II*, Binzel, R.P., Gehrels, T., and Mattews, M.S., Eds., Tucson: Univ. Arizona Press, 1989, pp. 921–945.

Betekhtin, A.G., *Kurs mineralogii* (Course of Mineralogy), Moscow: Gos. izd. geolog. lit., 1951.

Burns, R.G., *Mineralogical Applications of Crystal Field Theory*, New York: Cambridge Univ. Press, 1993.

Bus, S.J. and Binzel, R.P., Phase II of the small main-belt asteroid spectroscopic survey. A feature-based taxonomy, *Icarus,* 2002b, vol. 158, pp. 146–177.

Bus, S.J. and Binzel, R.P., Phase II of the small main-belt asteroid spectroscopic survey. The observations, *Icarus*, 2002a, vol. 158, pp. 106–145.

Busarev, V.V., Spectrophotometry of atmosphereless celestial bodies of the solar system, *Solar Syst. Res.*, 1999, vol. 33, pp. 120–129.

Busarev, V.V., Hydrated silicates on asteroids of M-, S-, and E-types as possible traces of collisions with bodies of the Jupiter growth zone, *Solar Syst. Res.*, 2002a, vol. 36, no. 1, pp. 39–47.

Busarev, V.V. and Taran, M.N., On the spectral similarity of carbonaceous chondrites and some hydrated and oxidized asteroids, *Proc. "Asteroids, Comets, Meteors (ACM 2002)"*, Berlin: Techn. Univ. of Berlin, 2002b, pp. 933–936.

Busarev, V.V., Bochkov, V.V., Prokof'eva, V.V., and Taran, M.N., Characterizing 21 Lutetia with its reflectance spectra, in *The new ROSETTA Targets*, Colangeli, L., et al., Eds., Kluwer Acad. Publ., 2004, pp. 79–83.

Busarev, V.V., Volovetskij, M.V., Taran, M.N., Fel'dman, V.I., Hiroi, T., and Krivokoneva, G.K., Results of reflectance spectral, Mössbauer, X-ràу and electron microprobe investigations of terrestrial serpentine samples, *Proc. 48th Vernadsky-Brown Microsymposium on Comparative Planetology*, Moscow, 2008, Abstr. 6.

Busarev, V.V., Spectral investigations of asteroids 21 Lutetia and 4 Vesta as objects of space missions, *Solar Sys. Res.,* 2010, vol. 44, no. 6, pp. 507–519.

Busarev, V.V., Asteroids 10 Hygiea, 135 Hertha, and 196 Philomela: heterogeneity of the material from the reflectance spectra, *Solar Syst. Res.,* 2011, vol. 45, no. 1, pp. 43–52.

Calvin, W.M. and King, T.V.V., Spectral characteristics of iron-bearing phyllosilicates: Comparison to Orgueil (CI1), Murchison and Murray (CM2), *Met. Planet. Sci.,* 1997, vol. 32, pp. 693–701.

Cayrel de Strobel, G., Stars resembling the Sun, *Astron. Astrophys. Rev.*, 1996, vol. 7, pp. 243–288.

Chapman, C.R., McCord, T.B., and Johnson, T.V., Asteroid spectral reflectivities, *Astron. J.*, 1973, vol. 78, pp. 126–140.

Clark, B.E., Binzel, R.P., Howell, E.S., Cloutis, E.A., Ockert-Bell, M., Christensen, P., Barucci, M.A., DeMeo, F., Lauretta, D.S., Connolly, H., Soderberg, A., Hergenrother, C., Lim, L., Emery, J., and Mueller, M., Asteroid (101955) 1999 RQ36: spectroscopy from 0.4 to

2.4 lm and meteorite analogs, *Icarus*, 2011, vol. 216, pp. 462–475.

Cloutis, E.A., Hiroi, T., Gaffey, M.J., Alexander, C.M.O.D., and Mann, P., Spectral reflectance properties of carbonaceous chondrites: 1. CI chondrites, *Icarus*, 2011a, vol. 212, pp. 180–209.

Cloutis, E.A., Hudon, P., Hiroi, T., Gaffey, M.J., and Mann, P., Spectral reflectance properties of carbonaceous chondrites: 2. CM chondrites, *Icarus*, 2011b, vol. 216, pp. 309–346.

DeMeo, F.E., Binzel, R.P., Slivan, S.M., and Bus, S.J., An extension of the bus asteroid taxonomy into the near-infrared, *Icarus,* 2009, vol. 202, pp. 160–180.

De Sanctis, M.C., Combe, J.-Ph., Ammannito, E., and 18 coauthors, Detection of widespread hydrated materials on Vesta by the VIR imaging spectrometer on board the dawn mission, *Astrophys. J. Lett.,* 2012, vol. 758, p. L36.

Drake, M.J., Geochemical evolution of the eucrite parent body: possible nature and evolution of Asteroid 4 Vesta?, in *Asteroids*, Gehrels, T., Ed., Tucson: Univ. Arizona Press, 1979, pp. 765–782.

Duke, M.B. and Silver, L.T., Petrology of eucrites, howardites and mesosiderites, *Geochim. Cosmochim. Acta*, 1967, vol. 31, pp. 1637–1665.

Efemeridy malykh planet na 2010 god (Minor Planets Ephemeredes for 2010), Batrakov, Yu.V., et al., Eds., St. Petersburg: Nauka, 2009, pp. 246–250.

Ferguson, J. and Fielding, P.E., The origins of the colours of yellow, green and blue sapphires, *Chem. Phys. Lett.*, 1971, vol. 10, pp. 262–265.

Fornasier, S., Migliorini, A., Dotto, E., and Barucci, M.A., Visible and near infrared spectroscopic investigation of E-type asteroids, including 2867 Steins, a target of the Rosetta mission, *Icarus,* 2008, vol. 196, pp. 119–134.

Fornasier, S., Clark, B.E., Dotto, E., Migliorini, A., Ockert-Bell, M., and Barucci, M.A., Spectroscopic survey of M-type asteroids, *Icarus,* 2010, vol. 210, pp. 655–673.

Fornasier, S., Clark, B.E., and Dotto, E., Spectroscopic survey of X-type asteroids, *Icarus,* 2011, vol. 214, pp. 131–146.

Fornasier, S., Lantz, C., Barucci, M.A., and Lazzarin, M., Aqueous alteration on main belt primitive asteroids: results from visible spectroscopy, *Icarus*, 2014, vol. 233, pp. 163–178.

Gaffey, M.J., Bell, J.F., and Cruikshank, D.P., Reflectance spectroscopy and asteroid surface mineralogy, in *Asteroids II*, Binzel, R.P., Gehrels, T., and Mattews, M.S., Eds., Tucson: Univ. Arizona Press, 1989, pp. 98–127.

Gaffey, M.J. and Kelley, S., Mineralogical variations among high albedo E-type asteroids: implications for asteroid igneous processes, *Proc. 35th Lunar and Planet. Sci. Conf.*, Houston, 2004, Abs. #1812.

Grimm, R.E. and McSween, H.Y., Jr., Heliocentric zoning of the asteroid belt by aluminum-26 heating, *Science*, 1993, vol. 259, pp. 653–655.

Hardorp, J., The Sun among the stars, *Astron. Astrophys.*, 1980, vol. 91, pp. 221–232.

Hergenrother, C.W., Nolan, M.C., Binzel, R.P., and 13 coauthors, Lightcurve, color and phase function photometry of the OSIRIS-REx target asteroid (101955) Bennu, *Icarus*, 2013, vol. 226, pp. 663–670.

Khomenko, V.M. and Platonov, A.N., *Porodoobrazuyushchie pirokseny: opticheskie spektry, okraska i pleokhroizm* (Rock-Forming Pyroxenes: Optical Spectra, Color and Pleochroism), Kiev: Naukova dumka, 1987.

Korzhinskii, D.S., *Fiziko-khimicheskie osnovy paragenezisov mineralov* (Physical and Chemical Foundations of Minerals Coexisting), Moscow: USSR Acad. Sci., 1957.

Kurucz, R.L., New atlases for solar flux, irradiance, central intensity, and limb intensity, *Mem. Soc. Astron. Italiana Suppl.*, 2005, vol. 8, pp. 189–191.

Lazzarin, M., Magrin, S., Marchi, S., Dotto, E., Perna, D., Barbieri, C., Barucci, M.A., and Fulchignoni, M., Rotational variation of the spectral slope of (21) Lutetia, the second asteroid target of ESA *Rosetta* mission, *Mon. Notic. Roy. Astron. Soc.*, 2010, vol. 408, pp. 1433–1437.

Lazzaro, D., Angeli, C.A., Carvano, J.M., Mothé-Diniz, T., Duffard, R., and Florczak, M., S^3OS^2: the visible spectroscopic survey of 820 asteroids, *Icarus*, 2004, vol. 172, pp. 179–220.

Lebofsky, L.A., Sykes, M.V., Tedesco, E.F., Veeder, G.J., Matson, D.L., Brown, R.H., Gradie, J.C., Feierberg, M.A., and Rudy, R.J., A refined 'standard' thermal model for asteroids based on observations of 1 Ceres and 2 Pallas, *Icarus*, 1986, vol. 68, pp. 239–251.

Li, J.-Y., McFadden, L.A., Parker, J.Wm., Young, E.F., Stern, S.A., Thomas, P.C., Russell, C.T., and Sykes, M.V., Photometric analysis of 1 Ceres and surface mapping from HST observations*, carus*, 2006, vol. 182, pp. 143–160.

Loeffler, B.M., Burns, R.G., Tossel, J.A., Vaughan, D.J., and Johnson, K.H., Charge transfer in lunar materials: interpretation of ultraviolet-visible spectral properties of the Moon, *Geochim. Cosmochim. Acta*, 1974, vol. 3, suppl. 5: *Proc. 5th Lunar Conf.*, pp. 3007–3016.

Mattson, S.M. and Rossman, G.R., Ferric iron in tourmaline, *Phys. Chem. Minerals*, 1984, vol. 11, pp. 225–234.

McCord, T.B., Li, J.-Y., Combe, J.-P., and 26 coauthors, Dark material on Vesta from the infall of carbonaceous volatile-rich material, *Nature,* 2012, vol. 491, pp. 83–86.

McSween, H.Y., Jr., Ghosh, A., Grimm, R.E., Wilson, L., and Young, E.D., Thermal evolution models of asteroids, in *Asteroids III*, Bottke, W., et al., Eds., Tucson: Univ. Arizona Press, 2002, pp. 559–571.

Ockert-Bell, M.E., Clark, B.E., Sheppard, M.K., Isaacs, R.A., Cloutis, E.A., Fornasier, S., and Bus, S.J., The composition of M-type asteroids: synthesis of spectroscopic and radar observations, *Icarus,* 2010, vol. 210, pp. 674–692.

Perna, D., Kaňuchová, Z., Ieva, S., Fornasier, S., Barucci, M.A., Lantz, C., Dotto, E., and Strazzulla, G., Short-term variability over the surface of (1) Ceres: a changing amount of water ice?, *Astron. Astrophys.*, 2015, vol. 575, id L1.

Petrova, E.V. and Tishkovets, V.P., Light scattering by morphologically complex objects and opposition effects (a review), *Solar Syst. Res.*, 2011, vol. 45, no. 4, pp. 304–322.

Platonov, A.N., *Priroda okraski mineralov* (Nature of Minerals Coloring), Kiev: Naukova dumka, 1976.

Reddy, V., Le Corre, L., O'Brien, D.O., and 22 coauthors, Delivery of dark material to Vesta via carbonaceous chondritic impacts, *Icarus*, 2012, vol. 221, pp. 544–559.

Rivkin, A.S., Howell, E.S., Britt, D.T., Lebofsky, L.A., Nolan, M.C., and Branston, D.D., 3-μm spectrophotometric survey of M- and E-class asteroids, *Icarus*, 1995, vol. 117, pp. 90–100.

Rivkin, A.S., Howell, E.S., Lebofsky, L.A., Clark, B.E., and Britt, D.T., The nature of M-class asteroids from 3-μm observations, *Icarus*, 2000, vol. 145, pp. 351–368.

Rossman, G.R., Spectroscopic and magnetic studies of ferric iron hydroxy sulfates: intensificadion of color in ferric iron clusters bridged by a single hydroxide ion, *Am. Mineral.,* 1975, vol. 60, pp. 698–704.

Shepard, M.K., Clark, B.E., Ockert-Bell, M., and 10 coauthors, A radar survey of M- and X-class asteroids. II. Summary and synthesis, *Icarus,* 2010, vol. 208, pp. 221–237.

Shepard, M.K., Harris, A.W., Taylor, P.A., and 7 coauthors, Radar observations of asteroids 64 Angelina and 69 Hesperia, *Icarus*, 2011, vol. 215, pp. 547–551.

Taran, M.N. and Rossman, G.R., High-temperature, high-pressure optical spectroscopic study of ferric-iron-bearing tourmaline, *Am. Mineral.*, 2002, vol. 87, pp. 1148–1153.

Tedesco, E.F., Noah, P.V., Noah, M., and Price, S.D., IRAS minor planet survey V6.0, *NASA Planetary Data System,* IRAS-A-FPA-3-RDR-IMPS-V6.0, 2004.

Tholen, D.J., Asteroid taxonomic classifications, in *Asteroids II*, Binzel, R.P., Gehrels, T., and Mattews, M.S., Eds., Tucson: Univ. Arizona Press, 1989a, pp. 1139–1150.

Tholen, D.J. and Barucci, M.A., Asteroid taxonomy, in *Asteroids II,* Binzel, R.P., Gehrels, T., and Mattews, M.S., Eds., Tucson: Univ. Arizona Press, 1989b, pp. 298–315.

Thomas, P.S., Binzel, R.P., Gaffey, M.J., Storrs, A.D., Wells, E.N., and Zellner, B.H., Impact excavation on asteroid 4 Vesta: Hubble Space Telescope results, *Science*, 1997, vol. 277, pp. 1492–1495.

Thomas, P.C., Parker, J.Wm., McFadden, L.A., Russell, C.T., Stern, S.A., Sykes, M.V., and Young, E.F., Differentiation of the asteroid Ceres as revealed by its shape, *Nature,* 2005, vol. 437, pp. 224–226.

Zolensky, M.E., Weisberg, M.K., Buchanan, P.C., and Mittlefehldt, D.W., Mineralogy of carbonaceous chondrite clasts in HED achondrites and the Moon, *Met. Planet. Sci.*, 1996, vol. 31, pp. 518–537.

Translated by A. Kobkova